Modelling of chemo-mechanical behaviour of low-pH Concretes

Youssef El Bitouri, Laurie Buffo-Lacarrière, Alain Sellier, Xavier Bourbon

Modelling of chemo-mechanical behaviour of low pH concretes

Y. El Bitouri [a,*], L. Buffo-Lacarrière [a], A. Sellier [a], X. Bourbon [b]

[a] Université de Toulouse, UPS, LMDC (Laboratoire Matériaux et Durabilité des Constructions), 135 Avenue de Rangueil, 31077 Toulouse cedex 04, France
[b] Andra (Agence Nationale pour la gestion des Déchets RadioActifs), 1 Rue Jean Monnet, F-92290 Châtenay-Malabry, France

A B S T R A C T

A model of the chemo-mechanical evolution of low-pH cement is clarified in order to be used at a structural scale. The proposed phenomenological model is based on a multiphasic hydration model developed in previous studies to predict the risk of early age cracking of structures cast with blended cements. At later ages, the evolution of mechan-ical properties cannot be explained only by the pozzolanic reaction usually considered in hydration models (because portlandite is entirely consumed at early ages). At these ages, mineralogical analyses showed that the hy-dration of remaining anhydrous silicate continued to develop by consumption of calcium from hydrates with high C/S ratios (e.g. C–S–H produced by clinker hydration at early age). A model able to predict these chemical evolutions is thus proposed. It is based on the principle of chemical equilibrium between the solution and the solid phases in terms of calcium concentration. The impact of this chemical evolution on mechanical properties can then be pre-dicted with a better accuracy than with a classical hydration model. Finally the chemo-mechanical model is applied to the prediction of cracking of a large concrete element cast with a low pH based concrete.

Keywords:
Blended cement (D); Modelling (E); Mechanical properties (C); C–S–H (B); Cracking

1. Introduction

One of the main concerns in the context of deep geological disposal of radioactive waste is that all elements of the storage structure (clay barrier and concrete) should maintain their confinement properties. To meet this requirement, the concrete used must satisfy certain criteria. For example, in order to reduce chemical interactions with clay, the pH of the pore solution of the concrete must not exceed 11 [1]. In addition, to reduce thermal gradients that may develop in the massive elements, the binder must release only a small amount of heat during hydration. These requirements have led to the use of special binders called low-pH cements [2,3,4].

* Corresponding author. Tel.: +33 5 61 55 66 97; fax: +33 5 61 55 99 49.
E-mail address: youssef.elbitouri@cebec-btp.com (Y. El Bitouri).

The principle of formulating these binders is based on a "key" parameter. To obtain a pH less than 11, it is necessary for the total equivalent silica content of the binder to exceed 50% by mass [5]. The formulation of low-pH cements is therefore characterized by a high degree of Portland cement substitution (30 to 70%) by pozzolanic minerals (silica fume, fly ash) [4,6,7] and hydraulic minerals (blast furnace slag) [2]. This high equivalent silica content changes the cement hydration processes (kinetics and hydrate composition). In general, changes in the composition of the final hydrates are well reproduced by thermodynamic modelling [8] but, for coupling with a mechanical model used to assess cracking risk, the hydration kinetics needs to be better known.

The hydration processes of Portland cement are well established [9]. The main hydrates that form in hydrated Portland cement are "jennite-like" C–S–H (with a high C/S ratio of about 1.7), portlandite, ettringite, and AFm phases. According to the thermodynamic calculations performed by Lothenbach et al. [8], the high degree of substitution of Portland cement by mineral additions such as slag or fly ash leads to the total consumption of portlandite to form "tobermorite-like" C–S–H (with low C/S ratio of about 1). However, a large amount of silica fume remains unhydrated in the short term. After the initial fast hydration process, the surplus silica progressively reacts with the high calcium C–S–H to form more low calcium C–S–H [7]. The stoichiometry of hydrates will therefore vary depending on the reaction of the silicate in the anhydrous phases. X-ray microanalyses of different low-pH cements performed by Bach et al. [10] illustrate this observation. It therefore appears that the evolution of the hydration of low-pH cements can be assessed by the evolution of the C/S ratio distribution of the paste. Previous studies have mainly focused on the characterization of hydrates, which did not allow the evolution of the C/S ratio distribution, and more especially the evolution of anhydrous material (present at the end of the first stage of hydration around 28 days), to be followed. The first aim of the present study was to perform X-ray microanalyses using energy dispersion spectroscopy at different maturities to compensate for the lack of results in the literature. This analysis had to include quantification of both hydrates and anhydrous material to estimate changes in the C/S ratio distribution.

Moreover, for a better prediction of the chemical and then mechanical properties of low-pH concrete, modelling of the stoichiometry variation during hydration was needed. There are microstructural models [11,12,13] that can take this stoichiometry variation into account but it is difficult to couple them with the structural models used in finite element codes. Furthermore, as the micromechanical properties of blended cement hydrates are not well known yet (for instance properties of low C/S C–S–H), the use of these microstructural models to compute mechanical property variation and to evaluate the cracking risk of large structures is not appropriate at the moment (for these specific binders).

In this paper, a phenomenological approach is used and hydration development and its consequences are predicted using a two-step model. At early age, an existing multiphase hydration model is used [14,20]. This model is well suited to the prediction of early age chemo-mechanical behaviour because it takes account of coupling between hydration development and water and temperature variations (which are needed to predict the strains that develop at early age in concrete in endogenous conditions). But this model assumes fixed stoichiometry for the hydrates produced by clinker and pozzolanic additions (such as silica fume). Consequently, it is not able to reproduce the long-term chemical evolutions observed in low-pH cement (hydration of silica fume and variation of C/S ratio in C–S–H). This is why, after 28 days (an arbitrarily chosen time, short enough for chemical evolutions to be considered as still negligible but long enough for the short-term reactions of hydration to be considered as relatively stabilized), a new model is proposed, which takes the long-term stoichiometry variation into account.

A mean hydration degree is then defined to link model results with mechanical properties. Finally, all the developments are used and coupled with a mechanical model in order to assess the risk of cracking of a structural element of a radioactive waste disposal structure. These calculations are carried out by coupling the chemical modelling with a mechanical model that considers the non-linear behaviour of hardening concrete (creep and damage).

2. Experimental study

2.1. Materials and methods

An experimental programme was carried out on one of the low-pH cements (ternary binder named T^L) containing 20% of Portland cement, 33% of silica fume and 47% of blast furnace slag. Table 1 shows the chemical composition of the raw materials used in the formulation of this binder. In previous studies on this binder [2,15], the authors focused on the analysis of the hydrated phase. The aim of the present experimental programme was to make a more detailed analysis including hydrates and anhydrous phases.

EDS-analysis was carried out on paste with a water/binder ratio of 0.5 (which corresponds to a water content of 570 l/m^3 of paste). The cement paste was mixed in a standard mortar mixer according to the following sequence: (i) pour water into mixer bowl, (ii) add dry components while stirring at low speed, (iii) mix at low speed for 3 min, then at high speed for 3 min. The samples were stored in hermetically sealed polypropylene recipients (2 cm in diameter × 5 cm deep) at 20 °C (in order to keep a high relative humidity). At each testing age, the hydration was stopped by quenching the materials in liquid nitrogen (at −196 °C), followed by sublimation of the ice in a freeze drier until constant sample weight was obtained.

The C/S ratio in the paste was determined by EDS analysis on polished cross sections observed with a scanning electron microscope (Philips XL PW6631/01 LaB6: filament accelerating voltage = 15 kV, interaction volume about 1 μm^3, and SEM-FEG). To take account of the heterogeneity of the paste, the observations were made with a magnification of ×300 on five sample zones. In each zone, five profiles were obtained to quantify the major elements with a spacing of 1 μm (Fig. 1). The size of the region analysed was about 600 × 450 μm. About 10,000 points were analysed along the red lines shown in Fig. 1.

2.2. Results and discussion

The EDS analyses were used to calculate the frequency of phases exhibiting specific C/S ratios (from 0 to 3 with a 0.02 step) at 3, 6 and 9 months of age. The histograms obtained experimentally are presented in Figs. 2, 3 and 4 with the mean square error between fitted curves and experimental histograms. The associated fitted parameters (modes, standard deviations and mode weights) are given in Table 2.

Table 1
Chemical composition (% weight) of binder constituents.

Chemical composition (% wt)	CEM I	Silica fume	Blast furnace slag
CaO	67.3	0.5	44
SiO_2	22.1	95	36.4
Al_2O_3	3.19	<0.20	10.7
Fe_2O_3	2.27	0.1	0.41
MgO	0.6	<0.20	7.25
MnO	<0.02	0.02	0.16
Na_2O	<0.20	<0.20	<0.20
K_2O	<0.05	0.34	0.22
TiO_2	0.18	<0.05	0.51
P_2O_5	0.24	0.09	<0.05
Sulphides	<0.10	<0.10	0.9
Sulphates	2.37	0.24	0.2
Loss on ignition (1000 °C)	1.64	2.21	<0.10
Specific surface area (m^2/g)	0.35	22	3.4
C/S ratio	3.04	0	1.21
Mean C/S ratio of binder	0.66		

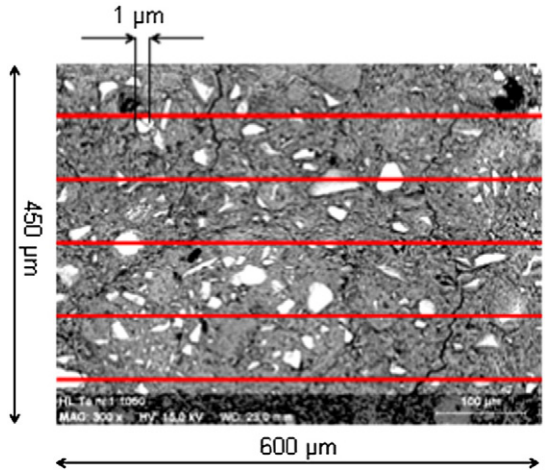

Fig. 1. Example of analysed area of the hydrated paste (magnification × 300, spacing 1 µm).

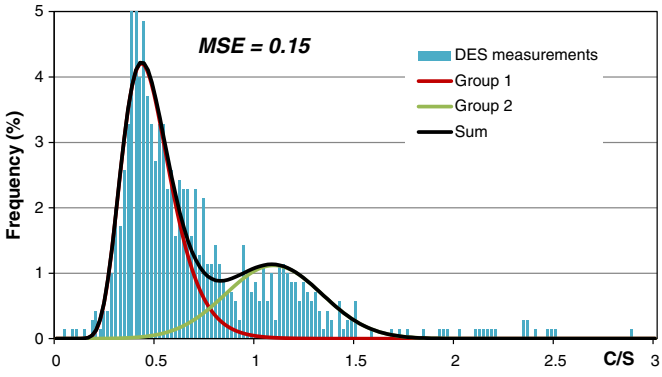

Fig. 2. C/S ratio frequency histogram for T^L paste after 3 months of curing at 20 °C.

To interpret these histograms we performed a deconvolution using two distribution laws. The calibration of the distribution laws was performed by minimizing the sum of the squared errors between the frequencies obtained experimentally for each C/S step and the value obtained by integrating the distribution law. The distribution laws chosen were normal laws, except for the results obtained at 3 months, for which the first distribution law (for lower C/S) was log-normal to avoid non admissible negative values.

For the 3-month results (Fig. 2), group 1, with low values of C/S ratio, can be attributed to a submicron mixture of unreacted silica fume and C–S–H with low C/S (produced by the "short-term" pozzolanic reaction of the silica fume). In the SEM observation, the EDS analysis showed that the silica fume (quite pure SiO_2) was dispersed among other hydrates

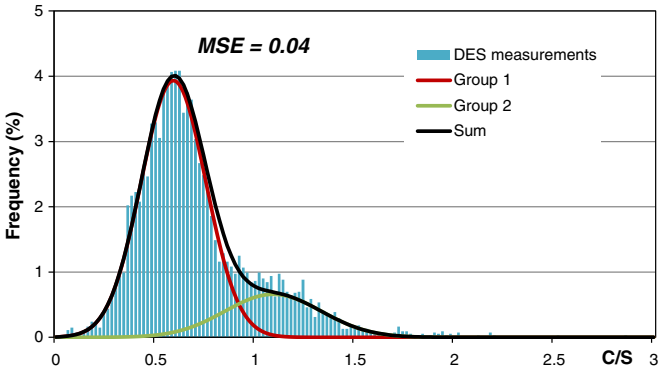

Fig. 3. C/S ratio frequency histogram for T^L paste after 6 months of curing at 20 °C.

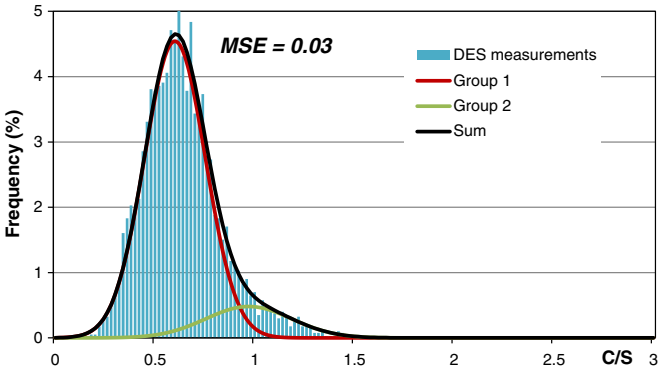

Fig. 4. C/S ratio frequency histogram for T^L paste after 9 months of curing at 20 °C.

(mainly the C–S–H) and the fineness of these particles, compared to the interaction volume of the EDS, did not allow observation of pure silica with a null C/S. This also explains why a Gaussian distribution law was not suitable. A log-normal law, being asymmetric, gave a better fit with the EDS measurement that could not detect pure silica fume alone. We can thus interpret the high frequency of solid with low C/S (group 1 with a mean value around 0.4 at 3 months) as an indicator of a large quantity of anhydrous silica fume. It was more difficult to identify the anhydrous part of slag because its C/S ratio (1.21) was very similar to that of C–S–H produced by its hydration when it was mixed with a small proportion of clinker [16,17,20] (equal to 1.19 at 28 days for the binder used in this study).

At 3 months, the second group (green law in Fig. 2) can thus be attributed to a mix of C–S–H produced by silica fume hydration, (with C/S around 1.15 [18,19], slag hydration (with C/S equal to 1.19 at 28 days for our binder) and clinker hydration (with C/S around 1.7) and residual anhydrous slag. Finally, at the other extremity, phases with C/S higher than 2 are representative of residual anhydrous phases of clinker (C3S and C2S). The small frequency of phases with high C/S ratios shows that these anhydrous phases are less present than remaining anhydrous silica fume and justify not introducing a distribution law for them.

By observing the results obtained at 6 and 9 months, we can see a progressive calcification of phases with lower C/S ratios and a decalcification of phases with high C/S (C–S–H created during short-term hydration). The mode weight of the first group increases with age while that of group 2 decreases. Moreover, C/S mode for group 2 decreases.

Unlike the results at 3 months, in both the 6- and 9-month results, group 1 can be reproduced by a normal law (symmetric law) as for high C/S ratios. This could indicate that C–S–H with very low C/S ratio can be seen by the EDS analysis. These C–S–H were created from the anhydrous silica fume (this last was not seen by the EDS analysis as noted in the 3-month results).

The chemical evolution model presented below takes these observations into account, in particular the continuation of the reaction of the silicate in anhydrous material with increasing age. The main mechanisms and full development of the model equations are presented first. Then, an application for ternary low-pH cement (T^L) is given.

Table 2
Modes, standard deviations and mode weights for distribution laws (except for group1 at 3 months, C/S mode and mean are the same).

	Group 1 (red curves)			Group 2 (green curves)		
	3 months	6 months	9 months	3 months	6 months	9 months
Mode weight	66%	80%	87%	34%	20%	13%
C/S mode	0.44	0.6	0.61	1.1	1.1	0.98
Standard deviation)	0.14	0.16	0.15	0.24	0.24	0.22

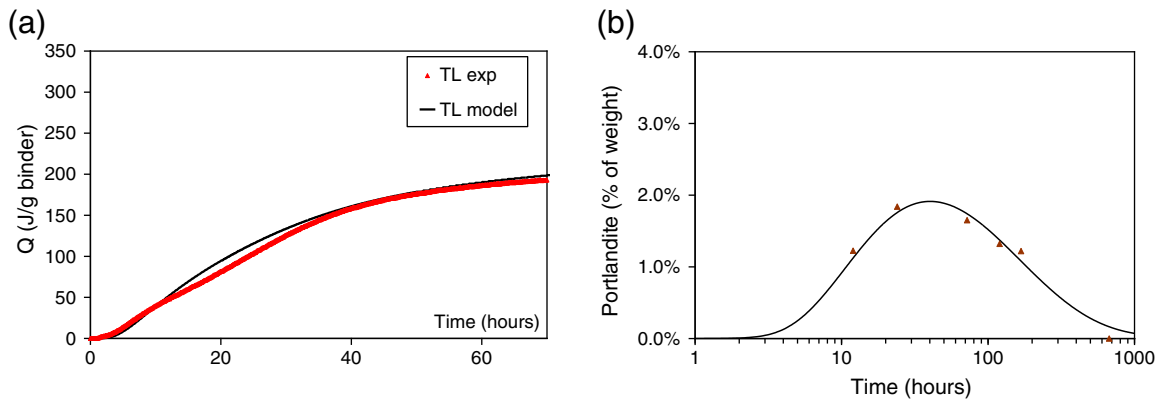

Fig. 5. Validation of the hydration model (Q is the quantity of heat per unit mass of binder).

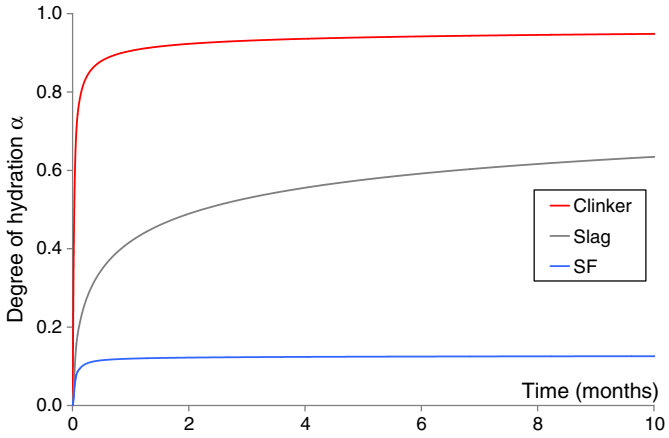

Fig. 6. Evolution of hydration degree of each component of low-pH cement (T^L).

3. Chemical evolution model

In order to predict the short-term development of the hydration for each component of low-pH cement, a multiphase hydration model developed previously was used up to 28 days [14,20]. The model predicts the evolution of the hydration degree of anhydrous phases (clinker, SF, slag, …) but, as kinetics is fast in the short term, it was assumed that the stoichiometry of the hydrates created did not evolve after their formation. The low-pH cement (named T^L) presented in Section 2.1 is used to illustrate the limits of this hydration model at later ages.

Fig. 5 shows the validation of the hydration model based on the heat release curve given by the Langavant test (Fig. 5-a) and the portlandite content (Fig. 5-b, the triangles represent experimental results found by Leung Pah Hang et al. [32]).

The model predicts the evolution of the hydration degree of each anhydrous phase (Fig. 6) and the quantity of each phase in the paste as presented in Tables 3 and 4. This mineralogical composition is predicted at 28 days and the water content of the paste at this age is 460 l/m^3 of paste.

Fig. 6 shows that the clinker is almost completely hydrated. The hydration of slag progresses slowly (latent hydraulic property). It should be noted that only 12% of silica fume had reacted at 28 days. The hydration model considers that silica fume reacts with portlandite to form C–S–H with a fixed C/S ratio (C/S = 1.15). As the amount of portlandite is negligible after 28 days (~3 mol/m^3), the pozzolanic reaction is stopped (in the hydration model). This explains the absence of change in the degree of silica fume reaction beyond 28 days, which is limited to about 0.1 (Fig. 6).

This hydration model, clarified to predict the risk of early age cracking induced by hydration exothermy in massive structures [21], is well suited to early ages, when reaction kinetics are fast enough to consider that variation of the stoichiometry of C–S–H can be neglected. However, for later ages, the experimental measurement presented in Section 2 showed that (1) this hypothesis of constant stoichiometry was no longer appropriate and (2) the remaining silica fume reacted even in the absence of portlandite. In fact, in the hydration model, the hydrates are not in equilibrium with the calcium content in the pore solution. A glance at Fig. 7 shows, for instance, that the aqueous calcium content corresponding to C–S–H produced by clinker is around 20 mmol/l while, for the C–S–H produced by slag or silica fume, it is around 5 mmol/l.

Table 3
Quantity of hydrated phases in paste predicted by the hydration model at 28 days.

	Clinker				Silica fume	Blast furnace slag		
	CH	$C_{1.7}SH_{2.1}$	AFm	Hexa	$C_{1.15}SH_{1.1}$	$C_{1.19}SH_{1.18}$	AFm	AFt
Quantity (mol/m^3 of paste)	3	761	61	33	702	1356	17	2

Table 4
Quantity of oxide or equivalent oxide in the residual anhydrous phases in paste.

	Clinker		Silica fume		Blast furnace slag	
	Initial	28 days	Initial	28 days	Initial	28 days
CaO (mol/m^3 of paste)	2752 (equivalent oxide)	303 (equivalent oxide)			4273 (equivalent oxide)	2608 (equivalent oxide)
SiO_2 (mol/m^3 of paste)	844 (equivalent oxide)	82 (equivalent oxide)	5893	5191	3300 (equivalent oxide)	1944 (equivalent oxide)

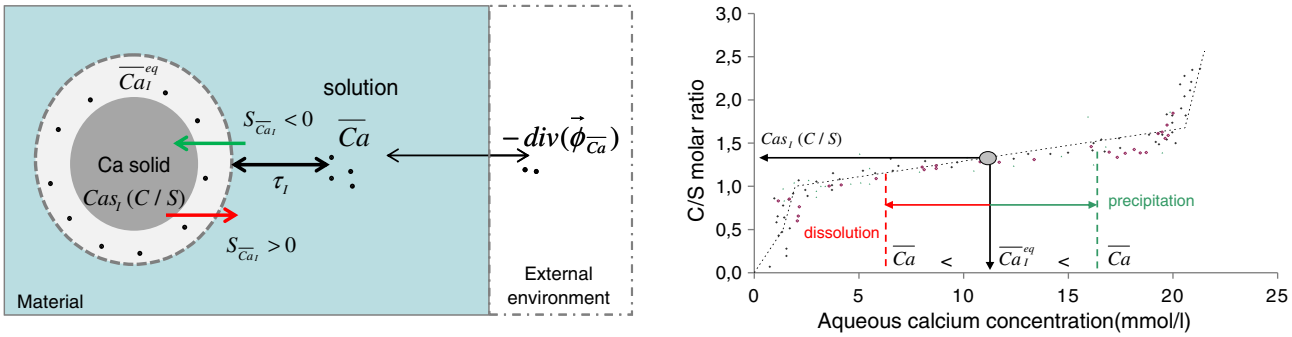

Fig 7. Local and macroscopic exchanges of calcium between solid phases and liquid.

It is disequilibrium that drives the exchange of calcium between solid phases and that explains the fact that C/S distribution changes from a multimodal distribution at 3 months to a single modal distribution at later ages.

3.1. Presentation of chemical evolution model

The model assumes that the evolution of calcium concentration alone in the liquid phase describes the chemical evolution of cement-based materials in the context of external calcium exchange (decalcification) [22–25] or of internal calcium exchange between the solid phases.

Local internal calcium exchange is due to a disequilibrium between the calcium content of the interstitial solution just around the solid phase $\overline{Ca}_I^{eq}$ (which is equilibrated with the solid phase following the local equilibrium diagram) and the calcium in the pore solution $\overline{Ca}$ [26,27] (Fig. 7). These local exchanges are represented, at macroscopic scale, in the mass balance equation (Eq. (1)) by a source of calcium $S_{\overline{Ca}_I}$ for each solid phase I.

$$\frac{\partial\left(w\overline{Ca}\right)}{\partial t} = -div\left(\vec{\phi}_{\overline{Ca}}\right) + \sum_I S_{\overline{Ca}_I} \tag{1}$$

where t is the time, w is the water content, and $\vec{\phi}_{\overline{Ca}}$ is the macroscopic calcium flow (in the case of a concentration gradient at macroscopic level).

The sink term $S_{\overline{Ca}_I}$ is calculated for each solid phase following the kinetics of dissolution/precipitation induced by local disequilibrium in the aqueous calcium content. The dissolution of solid calcium ($S_{\overline{Ca}_I} > 0$) occurs when the global calcium concentration in solution $\overline{Ca}$ is lower than the equilibrium concentration $\overline{Ca}_I^{eq}$ (Fig. 7).

This equilibrium concentration is controlled by the equilibrium diagram (Fig. 7) for silicate phases such as C–S–H and depends on the C/S of the phase. For calcium oxide in the anhydrous clinker and slag, and in portlandite, it occurs if the calcium concentration is less than 22 mmol/l. For aluminates (AFm and AFt), we assume that the dissolution of their solid calcium occurs progressively between 19 and 2 mmol/l. Calcium released by the dissolution of anhydrous clinker and slag, and by aluminates (AFm, AFt) will then be fixed by the siliceous phases (for which $\overline{Ca}$ is greater than $\overline{Ca}_I^{eq}$).

As the kinetics of dissolution/precipitation reactions depend not only on the chemical equilibrium but also on the calcium diffusion kinetics in the material at microscopic scale [24] the following equation is proposed.

$$S_{\overline{Ca}_I} = \frac{1}{\tau_I}\left(\overline{Ca}_I^{eq} - \overline{Ca}\right) \tag{2}$$

The function τ_I describes the delay of dissolution/precipitation reactions due to the micro-diffusion of calcium. This micro-diffusion, like diffusion at macro scale, is affected by the water content and the temperature. But it is also affected by the ability of calcium and water to move through the hydrates to reach anhydrous phases. The characteristic time is thus defined as follows:

$$\tau_I(t) = \tau_{28} \cdot g(w) \times h(T) . f_I^i\left(\frac{C}{S}\right) \tag{3}$$

In this equation, τ_{28} is a characteristic time calculated analytically in order to respect the continuity of the hydration kinetics at 28 days (given by the multiphase short-term hydration model).

The function g(w) reflects the fact that, when the water content (w) decreases, the kinetics of dissolution–precipitation reactions also decreases (Fig. 8). For this, the following expression is used:

$$g(w) = \frac{w_{28}}{w} \tag{4}$$

where w is the water content (m^3 (of water)/m^3 (of material)), w_{28} is the water content at 28 days provided by the hydration model. The

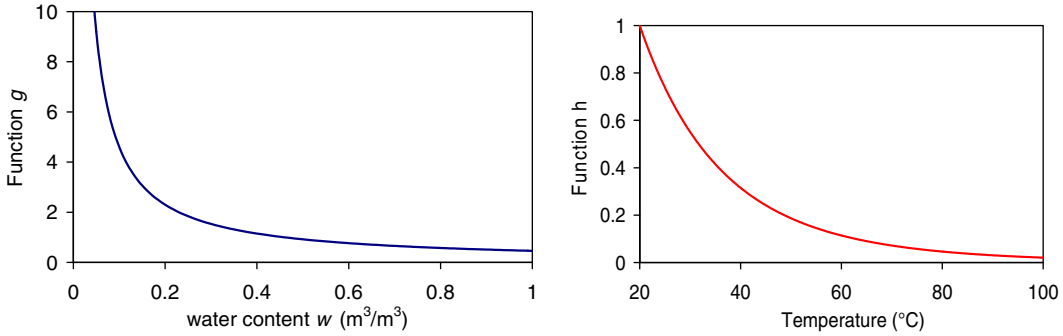

Fig. 8. Illustration of modelled effect of water and temperature on characteristic time.

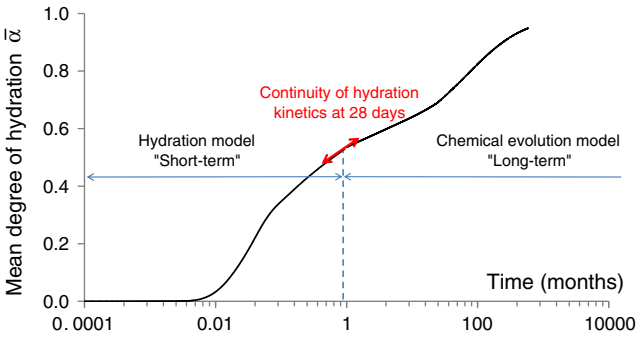

Fig. 9. Evolution of the mean degree of hydration for low pH cement T^L.

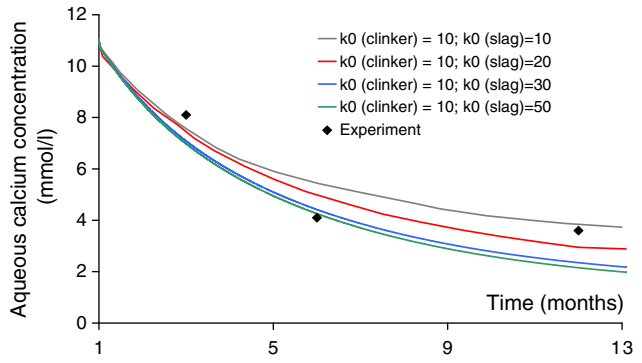

Fig. 10. Evolution of aqueous calcium concentration (mmol/l) for low pH cement T^L.

Table 5
Model parameters.

Parameters identified to ensure continuity with hydration model			Fitting parameters	
w_{28}	T_{28}	τ_{28}	k_0 (clinker)	k_0 (slag)
0.46 m^3/m^3	293 K	11 h	10	20

simple form chosen allows the reaction to be stopped in the absence of water.

The function h (Fig. 8) reflects the effect of temperature on the micro-diffusion kinetics (the effect on the solubility of hydrates is not yet taken into account, but should be). This effect can be described by an Arrhenius law, as has been proposed and validated experimentally by Peycelon et al. [28], with an activation energy E_d^a of 44 kJ/mol:

$$h(T) = \exp\left(\frac{E_d^a}{R}\left(\frac{1}{T} - \frac{1}{T_{28}}\right)\right) \quad (5)$$

where: T is the temperature (in K) and T_{28} is the temperature reached at 28 days (293 K) and predicted by the hydration model.

The function f describes the water accessibility to anhydrous material (clinker or slag). In fact, this accessibility can be affected by the formation of a new layer of hydrates surrounding the anhydrous phases. For anhydrous phases (clinker and slag), this function, initially equal to 1, increases progressively as the connection to the pore solution of new layers of hydrates created on the surface is reduced. On the other hand, for hydrates (present at 28 days), it is assumed that this new layer does not change their initial accessibility significantly and keeping the function f equal to 1 is therefore an acceptable approximation. Reactions of anhydrous phases are thus delayed by the effect of this new layer, except for the silica fume, for which the function f is also kept equal to 1. As its specific surface area is higher than that of clinker and slag, the silica fume, if it is well dispersed, is mixed with hydrates. We consequently consider that the function f concerns only residual anhydrous components of clinker and slag.

To take the effect of the new layer of hydrates (formation of C–S–H) into account, the function f evolves according to the increase of the progressive hydration of silicate present in the clinker and slag remaining at 28 days. As the water accessibility is managed by diffusion, an exponential function is chosen [14,20]. As the hydration progresses with the quantity of calcium bound in the new C–S–H created, the function is expressed according to the C/S ratio of new C–S–H:

$$f_l^i\left(\frac{C}{S}\right) = \exp\left(k_0^i \times \int \frac{\partial}{\partial t}\left(\frac{C}{S}\right) dt\right). \quad (6)$$

In this function, k_0^i is a fitting parameter for each anhydrous phase (i = clinker, slag). The method of determining the parameters τ_{28} and k_0^i will be explained in Section 4.1.

3.2. Definition of a mean degree of hydration for mechanical property evolution

In the case of blended cements, it is impossible to separate the contribution of the cement clinker and the additions to the development of mechanical properties, because they react together. A simplified approach consists of modelling the evolution of the mechanical properties with empirical laws by using a global variable for hydration. It should be noted that a homogenization approach [29,30] is also suitable for predicting the evolution of mechanical properties during hydration but it is not easy to implement in the case of low-pH cements because the mechanical properties of the great variety of hydrates created during the long-term chemical evolution are not known. So, the approach based on empirical laws [31] has the advantage of simplicity.

Concerning low pH cements, the definition of a global degree of hydration is needed. The chemical evolution model predicts the formation of new C–S–H by the progressive calcification of the unhydrated silicate and the decalcification of hydrates present at 28 days (Fig. 12,

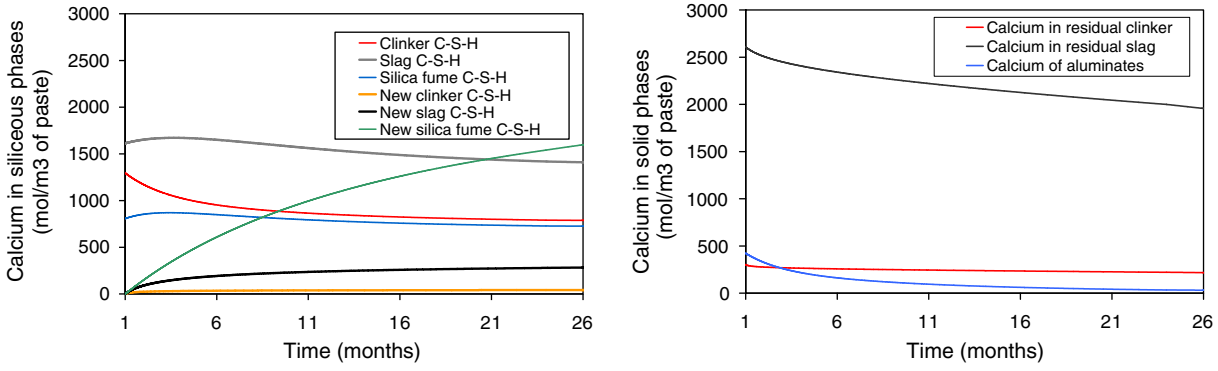

Fig. 11. Evolution of calcium in solid phases (siliceous phases on the left, aluminates and anhydrous calcium on the right).

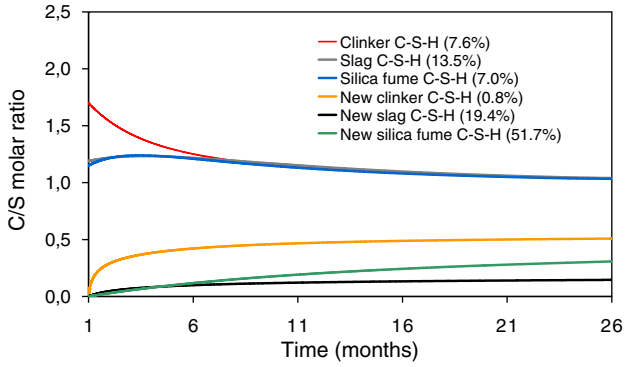

Fig. 12. Evolution of C/S ratio of siliceous phases.

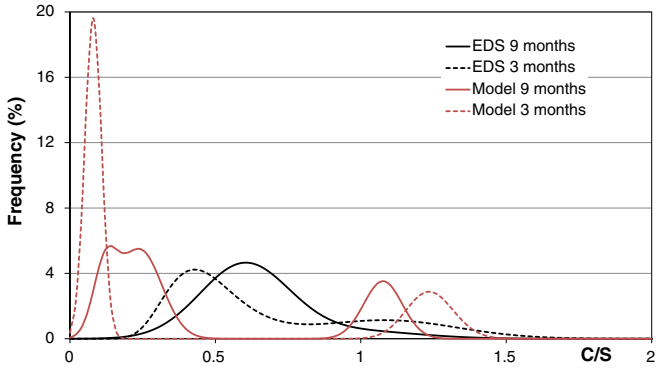

Fig. 13. C/S ratio frequency histogram for T^L paste.

Section 4.2). The new C–S–H formed after 28 days will contribute to the densification of the material and increase its cohesion. On the other hand, for the sake of simplicity, the moderate decalcification of phases having a high C/S ratio at 28 days is assumed not to affect the mechanical performance significantly (because, even with a low C/S, C–S–H remains a cohesion factor [22]). To take these considerations into account, a mean degree of hydration ($\overline{\alpha}$) is defined as follows (Eq. (7)):

$$\frac{\partial \overline{\alpha}}{\partial t} = \frac{1}{Ca^{total}} \sum_J \frac{\partial Ca_{SJ}}{\partial t} \tag{7}$$

where:

- $\overline{\alpha}$ is the mean degree of hydration,
- Ca^{total} is the total calcium content of the binder (mol/m^3 of material),
- Ca_{SJ} is the calcium content of the hydrated siliceous phases J (C–S–H) (mol/m^3 of material).

The calcium content variation of hydrated siliceous phases can be expressed as follows (Eq. (8)):

$$\frac{\partial Ca_{SJ}}{\partial t} = \underbrace{\frac{C}{S_J}\frac{\partial S_J}{\partial t}}_{a} + \underbrace{S_J \frac{\partial}{\partial t}\left(\frac{C}{S_J}\right)^+}_{b} \tag{8}$$

where:

- S_J is the molar content of hydrated siliceous phases (C–S–H) or unhydrated siliceous phase (remaining anhydrous silica fume for instance) (mol/m^3 of material),
- $\frac{C}{S_J}$ is the C/S molar ratio of the siliceous phase J (C/S starts >0 for C–S–H present at 28 days and from 0 for anhydrous silicate which will become the new C–S–H after 28 days),
- The symbol + means that only the calcification of the silicate is taken into account, it is assumed that the moderate decalcification at mid-term of C–S–H formed before 28 days does not affect the mechanical properties [22].

4. Application to low pH cement TL

In this section, the chemical evolution of the low-pH cement T^L is simulated in endogenous conditions. The composition given in Tables 3 and 4 is the input data for the chemical evolution model.

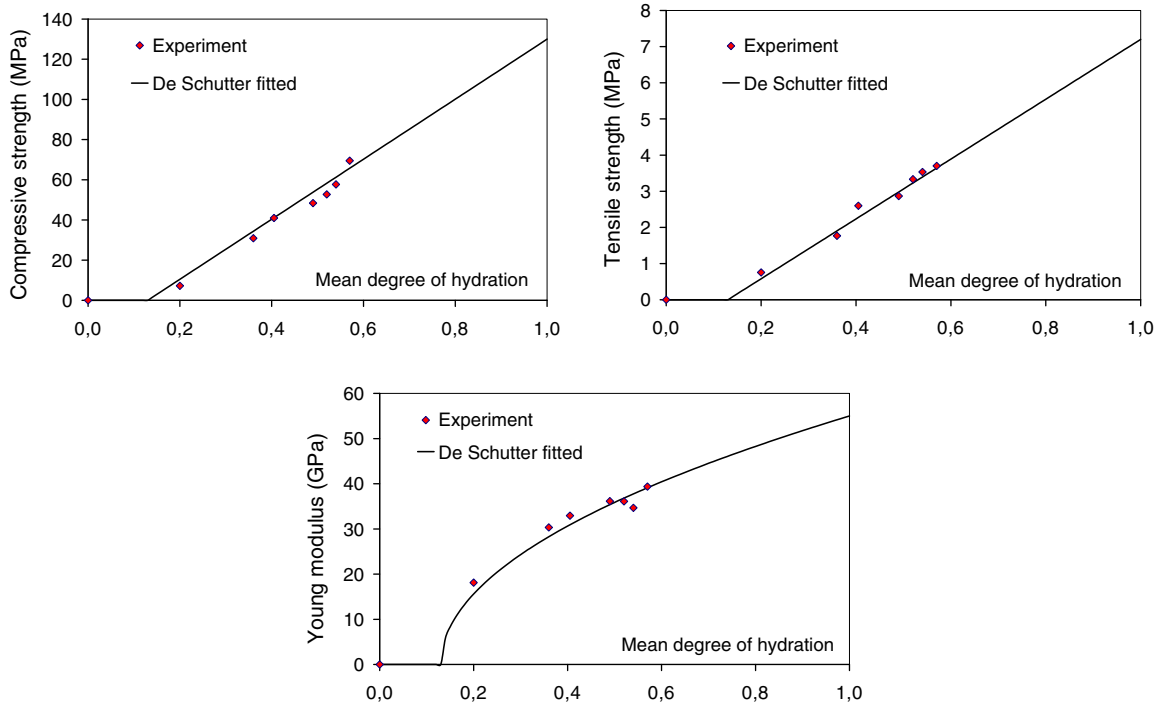

Fig. 14. Fitting of De Schutter's laws for low-pH concrete T^L (experiments from [32]).

Table 6
Parameters of De Shutter's law.

	Xith (MPa)	ki	$\overline{\alpha}_p$
R_c	130	1	0.13
R_t	7.2	1	
E_t	55	0.5	

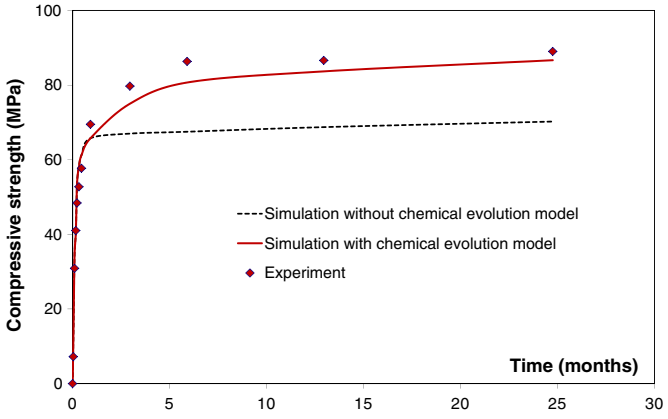

Fig. 15. Evolution of the mechanical properties without (dotted black curve) and with (red curve) the chemical evolution model (experiments from [32]).

4.1. Determination of model parameters

The characteristic time τ_{28} is calculated analytically in order to respect the continuity of the hydration kinetics at 28 days as illustrated in Fig. 9 and the parameter k_0^l, which controls the long-term kinetics, is estimated from the evolution of the aqueous calcium concentration.

The result of the fitting is presented in Fig. 10, where the triangles represent experimental results found by Bach [15] and the curve in red is the calibration result for fitting parameters k0 (slag and clinker) given in Table 5. The other curves highlight the influence of the fitting parameter k0 for slag. The characteristic time at 28 days is directly identified using the results of the hydration model in order to ensure kinetic continuity between the two models (Fig. 9). The only fitting parameters are k_0 for clinker and slag (Fig. 10). The water content and the temperature at 28 days are also given by the hydration model.

4.2. Evolution of mineral composition of hydrates

The main variable of our chemical evolution model is the calcium bound in solid phases; it is the variable used to characterize the mechanical evolution of the binder with time in the model. Fig. 11 illustrates the evolution of this variable for the siliceous phases (C–S–H formed during hydration and new C–S–H created during the chemical evolution process at higher ages) and for the other solid phases (aluminates for instance). On this figure, we can see that the model gives a good prediction of the qualitative evolution observed experimentally, with a decalcification of high C/S phases and the creation of new C–S–H by attraction of calcium by the silicates (mainly remaining anhydrous silica fume).

It should be noted that, in the model, the C3S and C2S in residual anhydrous clinker or slag is artificially separated into silicate and calcium ions. These anhydrous phases are thus not managed with their own C/S ratio but with a part of C/S = 0 (which created new C–S–H in Fig. 11 left) and pure calcium (which is progressively dissolved in Fig. 11 right).

For comparison with the histograms obtained experimentally, the results can also be expressed in terms of evolution of C/S ratios of siliceous solid phases (Fig. 12). For each phase the fraction of the phase in paste is also given.

In the model, for hydrates of each silicate, we considered only the mean C/S ratio of the total quantity of the phase. To ease comparison with the histogram envelope identified in Section 2, we distributed this mean C/S using normal laws. For each group (for TL binder we managed 6 silicate phases: 3 C–S–H produced by short term hydration of clinker, silica fume and slag, and 3 new C–S–H produced by complementary hydration of silicate in the remaining anhydrous phases), a standard variation around 0.05 was used. The mode weight associated with each mean C/S was the fraction of the corresponding solid phase calculated by the model. The histogram envelopes obtained are compared with the experimental ones in Fig. 13.

The model qualitatively reproduces the mineralogical evolution of paste between 3 and 9 months. A small proportion of the differences between experimental and model results can be explained by the fact that silicate anhydrous phases in clinker and slag are artificially separated in the model into pure calcium (with infinite C/S) and pure silica (with C/S of zero at 28 days). A part of the phases included in group 1 for model results is thus seen in group 2 for experimental results (slag particles with a mean C/S around 1.2).

But the main cause of the difference is the smoothing of the distribution induced by the experimental procedure (volume interaction of EDS and incapacity to "see" pure silica fume due to its small size compared to the zone investigated by the EDS, as explained in Section 2). The experimental distribution covers a lower range of C/S and exhibits larger modes (because the result of 1 measurement is the mean of several species).

Thus a quantitative validation of EDS analyses is not possible. As the chemical evolution model is designed to predict the evolution of the mechanical properties of these specific binders, the quantitative validation was performed indirectly with the mechanical properties.

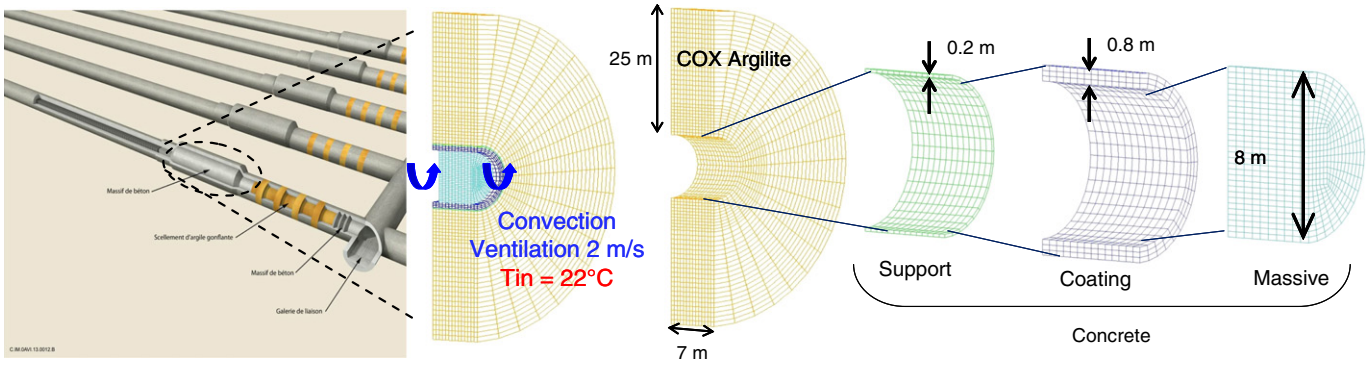

Fig. 16. The nuclear waste disposal structure (sealing system).

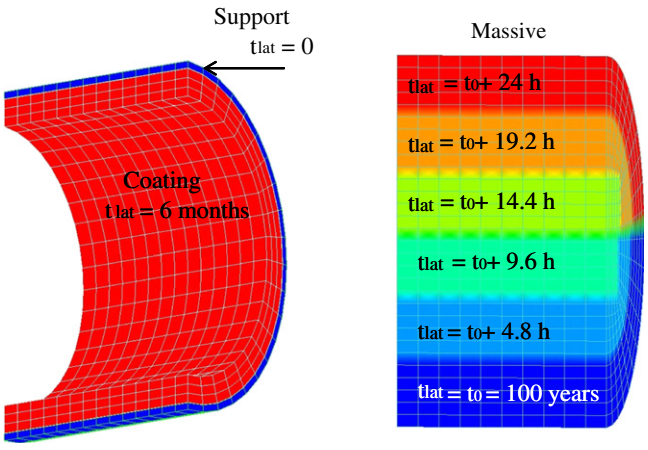

Fig. 17. Timing of the implementation of the various elements.

Table 7
Concrete formulation.

Material	Content (kg/m^3)
CEM I	76
Silica fume	123
Slag	180
Gravel	949
Sand	855
Effective water	152

4.3. Evolution of mechanical properties

To determine how the mechanical properties changed during chemical evolution (short-term hydration and complementary hydration after 28 days), the following empirical laws proposed in [31] were used:

$$X_i(\overline{\alpha}) = X_{ith}\left(\frac{\overline{\alpha}(t)-\overline{\alpha}_p}{1-\overline{\alpha}_p}\right)^{k_i} \quad (9)$$

where:

- $\overline{\alpha}$ is the mean degree of hydration previously defined according to the calcium content of solid phases by Eq. (7),
- R_{cth}, R_{tth} and E_{th} are, respectively, the theoretical compressive strength, tensile strength and Young modulus reached if $\overline{\alpha} = 1$,
- $\overline{\alpha}_p$ is the mean degree of hydration that corresponds to the mechanical threshold for percolation (calibration parameter identical for all mechanical properties considered),
- k_c, k_t and k_e are the calibration parameters, which depend on the type of cement and the concrete composition.

The mechanical experiments performed by Leun Pah Hang et al. [32] from casting to 28 days were used to calibrate the De Schutter's law parameters. Fig. 14 shows the result of this calibration. The parameters are shown in Table 6.

In order to validate the chemical evolution model, we simulated the evolution of compressive strength after 28 days using the parameters identified up to 28 days (Table 6). Fig. 15 clearly shows that the chemical evolution model (used instead of the short-term hydration model after 28 days) allows the evolution of mechanical properties to be better taken into account by predicting a higher hydration degree after 28 days.

The knowledge of how the mechanical properties of the low pH concrete T^L change during chemical evolution was subsequently used to calculate the risk of a structure element cracking during the first three months after casting.

4.4. Applicability at structural scale (radioactive waste storage structure)

The models presented in Section 3 were used to assess the risk of cracking of a massive structure d. The cracking risk studied was due to the temperature rise during the hydration. The structure studied was the sealing system of the nuclear waste disposal structure (Fig. 16). The storage structure is located 500 m deep in Callovo Oxfordian argillite. It consists of a 20-cm-thick support wall implemented just after excavation, an 80-cm-thick coating wall implemented 6 months after excavation, and a massive containment wall implemented 100 years after excavation. Given the massive nature of the latter, the technical implementation could have a significant impact on the temperatures developed during hydration, and hence the thermal strains induced at early age. The option considered here is progressive vertical casting (from bottom to top) in 24 h. To forecast the temperature in the structure, not only the concrete but also the soil had to be modelled, as heat transfers by conduction are allowed between the two materials and can significantly modify the temperature field.

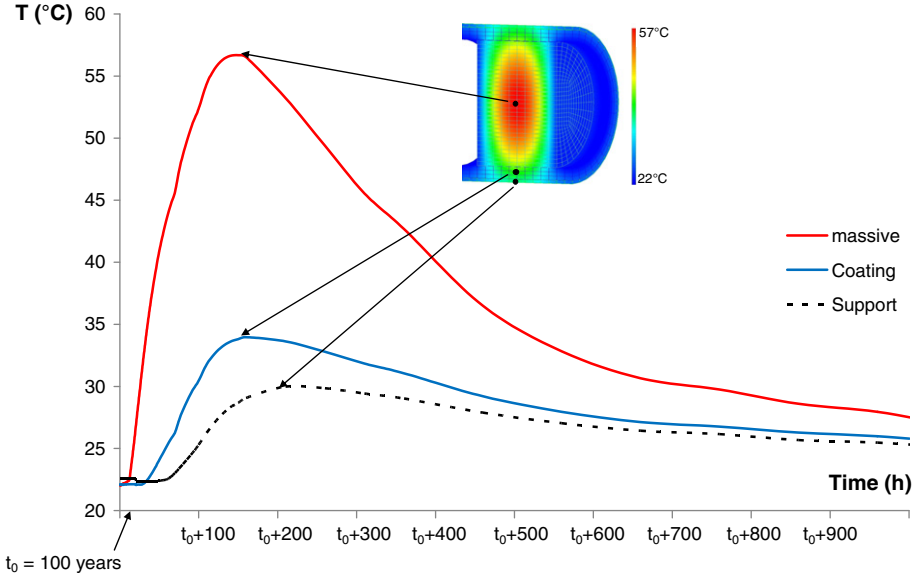

Fig. 18. Temperature variations for different points of the structure.

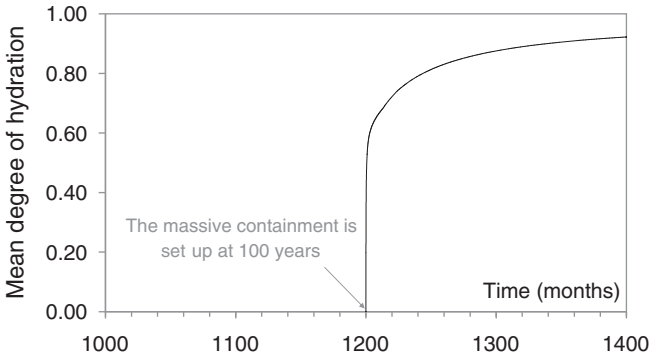

Fig. 19. Evolution of the mean degree of hydration for the massive containment (t_0 = 1200 months).

To simulate the behaviour of the structure, the timing of the implementation of the various elements (support wall, coating wall and containment wall) was taken into account by means of a latency time (Fig. 17). This latency time, defined previously by Kolani [33] to represent the delay effect induced by certain super-plasticizers (retarders) on cement hydration, was used as a numerical tool to delay casting in this study. The idea was to block the hydration of the element, as the latter had not been set up. This avoided having to resort to a complex mesh of the structure. Fig. 17 shows the latency time defined for each element.

For the calculation of the storage structure, the "short-term" hydration model and the "long-term" chemical evolution model were used to predict the development of the low-pH concrete (T^L) hydration. Then, using the chemo-mechanical coupling, a mechanical model was used to assess the risk of cracking due to the consequences of chemical evolution (heat release and variations in mechanical properties). The mechanical model previously developed by Sellier et al. [34,35] was used. This model consists of a rheological model for delayed strains (creep, shrinkage) coupled with an orthotropic damage model. The concrete formulation is presented in Table 7.

The calculations on the structure presented in Fig. 16 were performed by implementing the model in the 3D finite element code CASTEM2012 [36] (12,120 cubic elements, calculation time with a single processor: 12 h).

Fig. 18 illustrates temperature variation versus time for different points of the structure after the setting up of the massive block. The temperature, initially 22 °C, increases gradually to reach a maximum of 57 °C in the core of the massive block. This temperature rise is due to the heat released during hydration of the concrete. Furthermore, there is a thermal gradient between the core of the massive wall and the surfaces subjected to heat transfer by convection and conduction. This thermal gradient can cause cracking of the structure.

Fig. 19 shows the evolution of the mean degree of hydration of the massive block (set up at 100 years). The mean degree of hydration was calculated with the short-term hydration model, then with the chemical evolution model after 28 days.

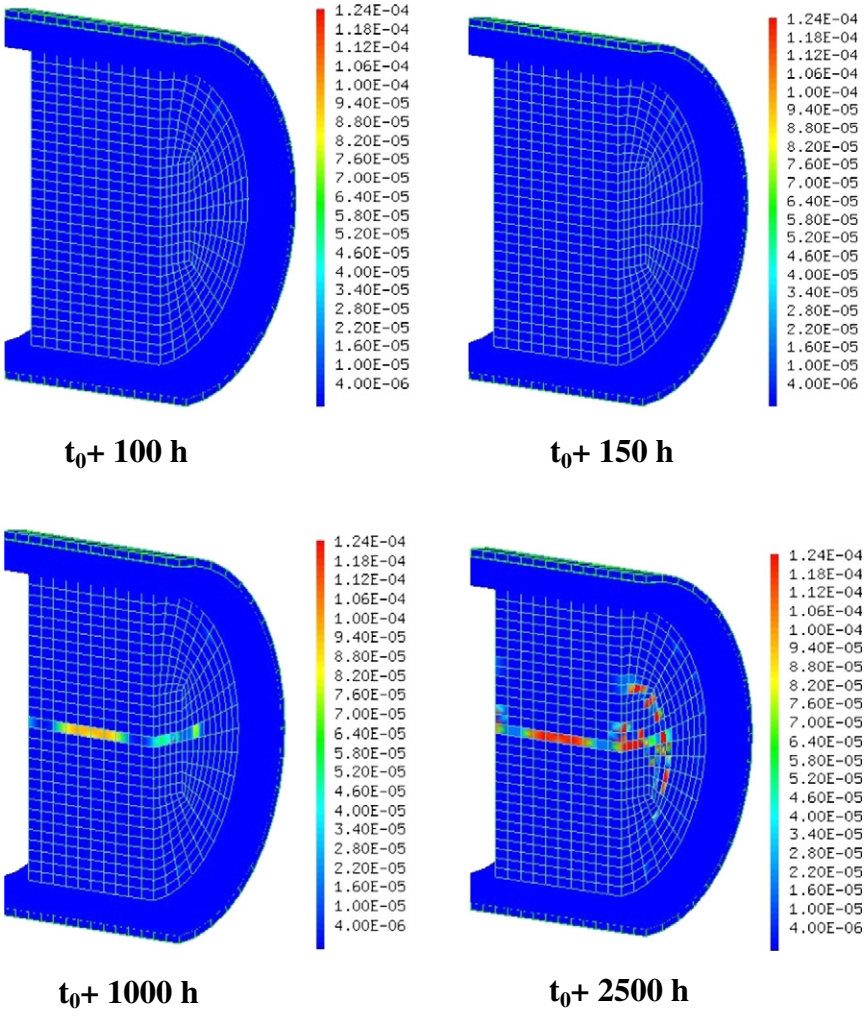

Fig. 20. Field of crack opening (m).

Fig. 20 shows the crack opening field. During the temperature rise phase, the dilation of the core of the massive wall is blocked by the boundary conditions. This leads to a system of stresses characterized by compressive stresses on the core of the massive block, and tensile stresses on the surfaces. This distribution of stresses leads to diffuse micro-cracking. In contrast, the stress distribution is reversed during the cooling phase, when the contraction of the core of the massive block is blocked by the edges. Such blocking of the contraction of the core of the massive block could lead to the initiation of a localized crack as shown in Fig. 20. A way to avoid this crack would be to optimize the casting process, in order to limit the temperature rise and so prevent thermal shrinkage gradients. This optimization could be performed by Andra using the proposed models.

5. Conclusions

A model predicting the hydration development of low-pH cements has been proposed. Based on the "solid-solution" principle, it assumes that the micro-diffusion of calcium plays a major role in explaining how the different C/S ratios of initial C–S–H all tend towards a medium stabilized value. This model is able to predict the hydration development beyond 28 days. The short-term hydration development is predicted by the multiphase hydration model previously proposed by Buffo-Lacarrière et al. [14]. The proposed complementary model can predict the residual silicate hydration qualitatively observed with the EDS-analysis. A hydration degree adapted to this type of cement was then defined. This variable was useful to consider the evolution of mechanical properties during hydration from short (<28 days in our case) term to long term. The prediction of the evolution of mechanical properties after 28 days shows that the chemical evolution model is needed for this kind of highly substituted binders, which exhibit a significant increase of mechanical properties at higher ages than clinker cement based concretes. Finally, the model was applied to a massive element of a radioactive-waste storage structure. It allowed to highlight a cracking risk if the casting chronology was too fast, and can now be used by Andra to optimize its building process in order to avoid the risk of cracking.

Acknowledgements

The authors acknowledge the technical and financial support of ANDRA (Agence Nationale pour la gestion des Déchets RadioActifs) (Andra n° 052231).

References

[1] ANDRA, 2005 Report on Clay—Evaluating the Feasibility of a Geological Repository in Clay FormationISBN: 2–951-0108-8-5 2005 238.
[2] M. Codina, C. Cau-dit-Coumes, P. Le Bescop, J. Verdier, J.P. Ollivier, Design and characterization of low-heat and low-alkalinity cements, Cem. Concr. Res. 38 (2008) 437–448.
[3] M.N. Gray, B.S. Shenton, For better concrete, take out some of the cement, Proc. 6th ACI/CANMET Symposium on the Durability of Concrete, May 31 to June 5 1998 (Bangkok, Thailand).
[4] T. Fries, H. Weber, V. Wetzig, Low-pH shotcrete field tests on apalinus clay samples, R&D on Low-pH Cement for a Geological Repository, 3rd workshop, Paris Jun 2007, pp. 13–14.
[5] C. Cau-Dit-Coumes, S. Courtois, D. Nectoux, S. Leclercq, X. Bourbon, Formulating a low-alkalinity, high-resistance and low-heat concrete for radioactive waste repositories, Cem. Concr. Res. 36 (2006) 2152–2163.
[6] M. Vuorio, J. Hansen, Long-term safety and durability related studies on low-pH grouting materials, R&D on Low-pH Cement for a Geological Repository, 3rd workshop, Paris Jun 2007, pp. 13–14.
[7] J.L. García Calvo, M.C. Alonso, A. Hidalgo, L.L. Fernàndez, Development of low-pH cementitious materials for HLRW repositories: resistance against ground water aggression, Cem. Concr. Res. 40 (2010) 1290–1297.
[8] B. Lothenbach, K. Scrivener, R.D. Hooton, Supplementary cementitious marterials, Cem. Concr. Res. 41 (2011) 1244–1256.
[9] H.F.W. Taylor, Cement Chemistry, second ed. Thomas Telford Publishing, London, 1997.
[10] T.T.H. Bach, C. Cau Dit Coumes, I. Pochard, C. Mercier, B. Revel, A. Nonat, Influence of temperature on the hydration products of low pH cements, Cem. Concr. Res. 42 (2012) 805–817.
[11] E.J. Garboczi, D.P. Bentz, Fundamental computer simulation models for cement-based materials, in: J. Skalny, S. Mindess (Eds.), Materials Science of Concrete II, American Ceramic Society, Westerville, OH 1991, pp. 249–273.
[12] K. Van Breugel, Simulation of Hydration and Formation of Structure in Hardening Cement Based MaterialsPhD thesis University of Delft, Netherlands, 1997.
[13] X. Liu, Y. Guang, G. De Schutter, Y. Yuan, Simulation of the microstructure formation in hardening self-compacting cement paste containing limestone powder as filler via computer-based model, Mater. Struct. 46 (2013) 1861–1879.
[14] L. Buffo-Lacarrière, A. Sellier, G. Escadeillas, A. Turatsinze, Multiphasic finite element modeling of concrete hydration, Cem. Concr. Res. 37 (2007) 131–138.
[15] T.T.H. Bach, Evolution physico-chimique des liants bas-pH hydratés, influence de la température et mécanismes de rétention des alcalinsPhD thesis Université de Bourgogne, Dijon, France, 2010 (167 pp.).
[16] I.G. Richardson, G.W. Groves, The incorporation of minor and trace elements into calcium silicate hydrate (C–S–H) gel in hardened cement pastes, Cem. Concr. Res. 23 (1) (1993) 131–138.
[17] I.G. Richardson, Tobermorite/jennite- and tobermorite/calcium hydroxide-based models for the structure of C–S–H: applicability to hardened pastes of tricalcium silicate, β-dicalcium silicate, Portland cement, and blends of Portland cement with blast-furnace slag, metakaolin, or silica fume, Cem. Concr. Res. 34 (2004) 1733–1777.
[18] V. Waller, Relations entre composition des bétons, exothermie en cours de prise et résistance en compressionPhD thesis ENPC, Paris, France, 1999 (297 pp.).
[19] H. Justnes, Hydraulic binders based on condensed silica fume and slake lime, 9th International Congress on the Chemistry of Cement, New Delhi, vol. III 1992, pp. 284–290.
[20] B. Kolani, L. Buffo-Lacarrière, A. Sellier, G. Escadeillas, L. Boutillon, L. Linger, Hydration of slag-blended cements, Cem. Concr. Compos. 34 (2012) 1009–1018.
[21] L. Buffo-Lacarrière, A. Sellier, G. Escadeillas, A. Turatsinze, Numerical modelling of hardening concrete mechanical behaviour: application to the prediction of early age cracking risk for massive structures, Mater. Struct. vol. 44 (n°10) (2011) 1821–1835.
[22] B. Gérard, Contribution des couplages mécanique-chimie-transfert dans la tenue à long terme des ouvrages de stockage de déchets radioactifsPhD thesis ENS Cachan, Paris, France, and Université de Laval, Québec, Canada, 1996 (373 pp.).
[23] M. Mainguy, C. Tognazzi, J.M. Torrenti, F. Adenot, Modelling of leaching in pure cement paste and mortar, Cem. Concr. Res. 30 (2000) 83–90.
[24] D. Gawin, F. Pesavento, B. Schrefler, Modeling deterioration of cementitious materials exposed to calcium leaching in non-isothermal conditions, Comput. Methods Appl. Mech. Eng. 198 (2009) 3051–3083, http://dx.doi.org/10.1016/j.cma.2009.05.005.
[25] A. Sellier, L. Buffo-Lacarrière, Chemo-mechanical modeling requirements for the assessment of concrete structure service life, J. Eng. Mech., 137, American Society of Civil Engineers 2011, pp. 625–633 (N°9).
[26] K. Fuji, W. Kondo, Heterogeneous of calcium silicate hydrate in water at 30 °C, J. Chem. Soc. Dalton Trans. 2 (1981) 645–651.
[27] G.L. Kalousek, Application of differential thermal analysis in a study of the system lime-silica-water, Third International Symposium on the Chemistry of Cement, London 1952, pp. 296–311.
[28] H. Peycelon, C. Blanc, C. Mazoin, Long term behaviour of concrete, Influence of temperature and cement binders on the degradation (decalcification/hydrolysis) in saturated conditions, Revue européenne de génie civil, vol. 10, 2006 (n°9).
[29] O. Bernard, F.J. Ulm, E. Lemarchand, A multiscale micromechanics-hydration model for the early age elastic properties of cement-based materials, Cem. Concr. Res. 33 (2003) 1293–1309.
[30] J.M. Torrenti, F. Benboudjema, Mechanical threshold of cementitious materials at early age, Mater. Struct. 38 (n°277) (2005) 299–304.
[31] G. De Schutter, L. Taerwe, Degree of hydration based description of mechanical properties of early age concrete, Mater. Struct. 29 (1996) 335–344.
[32] T. Leung Pah Hang, J. Verdier, T. Vidal, L. Buffo-Lacarrière, X. Bourbon, Hydration and properties of low pH concrete, Consec13, Nanjing, China, 2013.
[33] B. Kolani, Comportement au jeune âge des structures en béton armé à base de liants composés aux laitiersPhD thesis Université de Toulouse, France, 2012 (282 pp.).
[34] A. Sellier, L. Buffo-Lacarrière, Towards a simple and unified modelling of basic creep, shrinkage and drying creep of concrete, Eur. J. Environ. Civ. Eng. 13 (2009) 1161–1182 N°10.
[35] A. Sellier, G. Casaux-Ginestet, L. Buffo-Lacarrière, X. Bourbon, Orthotropic damage coupled with localized crack reclosure processing, Part I: Constitutive laws, Eng. Fract. Mech. 97 (2013) 148–167.
[36] Commissariat à l'Energie Atomique CEA — DEN/DM2S/SEMT, CASTEM2012, web page: http://www-cast3m.cea.fr/